ADVANCED ENERGY MATERIALS
www.advenergymat.de

www.MaterialsViews.com

Confined and Chemically Flexible Grain Boundaries in Polycrystalline Compound Semiconductors

Daniel Abou-Ras, Sebastian S. Schmidt, Raquel Caballero, Thomas Unold, Hans-Werner Schock, Christoph T. Koch, Bernhard Schaffer, Miroslava Schaffer, Pyuck-Pa Choi, and Oana Cojocaru-Mirédin*

Grain boundaries (GBs) in polycrystalline $Cu(In,Ga)Se_2$ thin films exhibit only slightly enhanced recombination, as compared with the grain interiors, allowing for very high power-conversion efficiencies of more than 20% in the corresponding solar-cell devices. This work highlights the specific compositional and electrical properties of $Cu(In,Ga)Se_2$ GBs by application of appropriate subnanometer characterisation techniques: inline electron holography, electron energy-loss spectroscopy, and atom-probe tomography. It is found that changes of composition at the GBs are confined to regions of only about 1 nm in width. Therefore, these compositional changes are not due to secondary phases but atomic or ionic redistribution within the atomic planes close to the GBs. For different GBs in the $Cu(In,Ga)Se_2$ thin film investigated, different atomic or ionic redistributions are also found. This chemical flexibility makes polycrystalline $Cu(In,Ga)Se_2$ thin films particularly suitable for photovoltaic applications.

1. Introduction

Thin-film solar cells exhibit high power-conversion efficiencies of up to more than 20%[1,2] using polycrystalline $Cu(In,Ga)Se_2$ absorber layers; the highest efficiencies have been achieved with Ga/([In]+[Ga]) ratios in these absorber layers of about 0.2–0.4.[3] Such device performances are astonishing in view of the average grain sizes of 0.5–1.5 μm in $Cu(In,Ga)Se_2$ layers,[4] which exhibit thicknesses of typically 2–3 μm, because the generated photocurrent passes on average at least one grain boundary (GB) on its path through the $Cu(In,Ga)Se_2$ absorber layer.

This fact gives rise to the assumption that the GBs in polycrystalline $Cu(In,Ga)Se_2$ thin-films are not detrimental to charge-carrier collection, or at least that this collection is not reduced substantially by enhanced recombination at GBs. Indeed, this assumption has recently been confirmed by means of electron-beam-induced current (EBIC) measurements, combined with electron backscatter diffraction (EBSD) on cross-sectional specimens from $Cu(In,Ga)Se_2$ solar cells.[5] The question remains: what makes the GBs in polycrystalline $Cu(In,Ga)Se_2$ thin-films so special, compared with those present in other photovoltaic materials, such as multicrystalline Si?[6] Since the scenario for GBs at the surface, with unsaturated dangling bonds, is expected to be different from those in the interior of the $Cu(In,Ga)Se_2$ thin-films, we emphasize the necessity to regard the surface and the volume GB scenarios separately, as has been outlined by Sadewasser et al.[7]

This work intends to highlight the nature of GBs in the volumes of polycrystalline $Cu(In,Ga)Se_2$ thin-films in completed solar cells with high power conversion efficiencies of about 15–16%. We also discern highly symmetric Σ3 and random GBs. In the present work, we will concentrate on the analysis of the latter GB type. Various characterisation techniques with subnanometer resolutions were applied: in-line electron holography[8,9] (also known as Fresnel contrast analysis[10]), and electron energy-loss spectroscopy (EELS) in a transmission electron microscope (TEM), as well as atom-probe tomography (APT). These three techniques were employed on the same $Cu(In,Ga)Se_2$ thin-film.

Dr. D. Abou-Ras, Dr. S. S. Schmidt, Dr. R. Caballero,[+]
Dr. T. Unold
Helmholtz-Zentrum Berlin für Materialien
und Energie GmbH
Hahn-Meitner-Platz 1, 14109 Berlin, Germany
E-mail: daniel.abou-ras@helmholtz-berlin.de
Prof. C. T. Koch[++]
Max-Planck Institute for Intelligent Systems
Heisenbergstr. 3, 70569 Stuttgart, Germany
Dr. B. Schaffer, Dr. M. Schaffer
SuperSTEM, STFC Daresbury Laboratories
Keckwick Lane, Warrington, WA4 4AD, UK
Dr. B. Schaffer
SUPA School of Physics and Astronomy
University of Glasgow
Glasgow, G12 8QQ, UK
Prof. H.-W. Schock, Dr. M. Schaffer
Department of Engineering
George Holt Building, Ashton Street, Liverpool, L69 3BX, UK
Dr. P.-P. Choi, Dr. O. Cojocaru-Mirédin
Max-Planck-Institut für Eisenforschung GmbH
Department of Microstructure Physics and Alloy Design
Max-Planck-Strasse 1, 40237 Düsseldorf, Germany
[+] Present address: Universidad Autónoma de Madrid, Departamento de Física Aplicada, C/Francisco Tomás y Valiente 7, 28049 Madrid, Spain
[++] Present address: Institute for Experimental Physics, Ulm University, 89069 Ulm, Germany

DOI: 10.1002/aenm.201100764

2. Materials and Methods

1.9 μm thick Cu(In,Ga)Se_2 thin films were deposited on DC-sputtered Mo-coated soda-lime glass via multi-stage coevaporation. In the first stage of the deposition process, Ga, In, and Se were evaporated sequentially at a nominal substrate temperature of T_{sub} = 330 °C. The consecutive deposition stages of the process were all performed at a nominal temperature T_{sub} = 525 °C. Cu–Se was coevaporated in stage two until the ratio [Cu]/([In]+[Ga]) was larger than 1. In stage three, In–Ga–Se were deposited simultaneously to produce Cu(In,Ga)Se_2 with overall ratio [Cu]/([In] + [Ga]) < 1. The Cu(In,Ga)Se_2 thin-films studied exhibited compositional ratios of [Cu]/([In] + [Ga]) = 0.88 and of [Ga]/([In] + [Ga]) = 0.26, as measured by X-ray fluorescence analyses. The solar cells were completed by chemical bath deposition of a CdS buffer layer (approximately 50 nm thick), an RF-sputtered ZnO/ZnO:Al bilayer front contact, and the evaporation of Ni/Al grids in order to facilitate current collection.

Cross-of solar cells were mechanically polished until they were about 20 μm thick and further thinned by use of a FIB to obtain TEM specimens transparent for 200 kV electrons. The reconstruction of the relative phase differences $\Delta\phi(x,y)$ in the object wave determined by use of inline electron holography was based on the acquisition of a through focal series with a set of 15 images by use of a Zeiss LIBRA 200FE TEM equipped with an omega-type energy filter. A nominal defocus step of 800–1200 nm between the individual images was adjusted. The actual defocus steps were fitted during the computational reconstruction of the object wave. Inelastically scattered electrons were filtered out by a 10 eV wide energy-selecting slit placed on the zero-loss region in the energy dispersive plane of the electron spectrometer. An objective aperture with radius of about 1.2 nm^{-1} was applied. A low-pass filter of the same size in Fourier space was applied on the acquired images of the through focal series before the reconstruction, to filter out noise. A magnification of about 135 000 was adjusted for the acquisition of the through focal series. Illumination angles (given by illumination apertures) smaller than nominally 50 μrad were chosen for the acquisition of the through focal series. These illumination angles emerged as optimal considering the trade-off between the highest possible degree of coherence of the incident electron beam and a reasonable signal-to-noise ratio of the images. As consequence, this also kept the generation of free charge-carriers by the electron beam within the Cu(In,Ga)Se_2 semiconductor as low as possible. The computational reconstruction of the object wave was performed by the procedure described by Schaffer et al.[11]

Focused ion beam prepared TEM specimens were sliced from working devices using FEI Helios NanoLab 600 DualBeam and Zeiss XBeam 1540 FIBs. The samples were precoated by a 60 nm carbon layer in an EMITEC K950X carbon coater and an adapted FIB in situ lift-out lamella preparation technique was applied, ensuring the suitability of the specimen for atomic resolution imaging and analysis at 100 kV. This procedure involves large Pt/C protection layers, initially higher tilting angles, an adjusted low-kV Ga milling at early preparation stages, and final Ga milling at 0.5 kV acceleration voltage.[11]

The EELS data was acquired using a NION UltraSTEM 100 microscope, equipped with a cold-FEG emitter, a C_5/C_3 aberration corrector, and a Gatan ENFINA spectrometer for EELS measurements. The microscope was operated at 100 kV with a convergence half-angle of 30 mrad, and an EELS collection half-angle of 31 mrad was selected by the spectrometer entrance aperture. Spectra were acquired at a 1 eV/channel dispersion covering the energy-loss range from 300 to 1640 eV. The CCD chip of the spectrometer was asymmetrically binned by 1 × 100 for higher readout speed and less readout noise. For the measurements, random GBs were identified by orientation contrast between grains and the non-planar interface between them. Such GBs were located in the thinnest specimen areas of 10 to 25 nm thickness, and the sample was then tilted to minimize the visible transition between both grains hence orienting the boundary parallel to the electron beam direction and minimizing geometric projection. To achieve a sufficient signal-to-noise ratio to reliably map concentration changes of Cu and Se, exposure times of at least 1 s per position were necessary. A special distributed-dose acquisition mode[12] was used to avoid beam damage during the measurement, averaging the signal over approximately 2 nm parallel to the GB.

APT samples were prepared by means of FIB (FEI Helios Nanolab 600) according to the lift-out procedure described by Miller et al.[13] In order to minimize Ga^+ beam damage, a low energy (5 keV) Ga beam was used at the final ion-milling stage. APT experiments were performed with a local electrode atom probe (LEAP™ 3000X HR, Cameca Instruments). These experiments were carried out applying laser pulses of about 532 nm wavelength, 12 ps pulse length, and an energy of 0.1 nJ per pulse at a repetition rate of 100 kHz. The specimen base temperature was about 60 K.

3. Results and Discussion

In-line electron holography in a TEM records the lateral variations of the amplitude and phase of the exit-plane electron wave function, after the interaction of the incident electron beam with the specimen (i.e., images containing amplitude and phase information as grey values). The lateral phase variation $\phi(x,y)$ is proportional to the variation in the projected electrostatic potential that an electron experiences when it travels trough the specimen.[14] The average potential can then be calculated using $\Delta V_{av}(x, y) = \frac{\varphi(x,y)}{\sigma t(x,y)}$ (Equation 1), where σ is an interaction constant depending on the acceleration voltage of the TEM. The parameter $t(x,y)$ is the specimen thickness at the region of interest determined by acquiring unfiltered and zero-loss-filtered TEM images with intensity distributions $I_u(x,y)$ and $I_0(x,y)$ and by applying[15] $t(\vec{r}) = \lambda_{mfp} \ln\left(\frac{I_u(x,y)}{I_0(x,y)}\right)$, where λ_{mfp} is the inelastic mean free path of the beam electrons in the specimen for a given collection angle of the spectrometer. **Figure 1** shows, as an example, distributions of the relative phase shift and the specimen thickness around a random GB in a Cu(In,Ga)Se_2 thin-film as well as of the resulting profile across the GB, which was extracted from the distribution of the average electrostatic potential, calculated by use of Equation 1.

The lateral variation of the averaged electrostatic potential (not to be confused with potential energy) can be considered as the sum of variations related to a lateral redistribution of free charge carriers, ΔV_{charge}, and to the mean-inner potential (MIP): $\Delta V_{av} = \Delta MIP + \Delta V_{charge}$. The MIP is due to the distribution of all

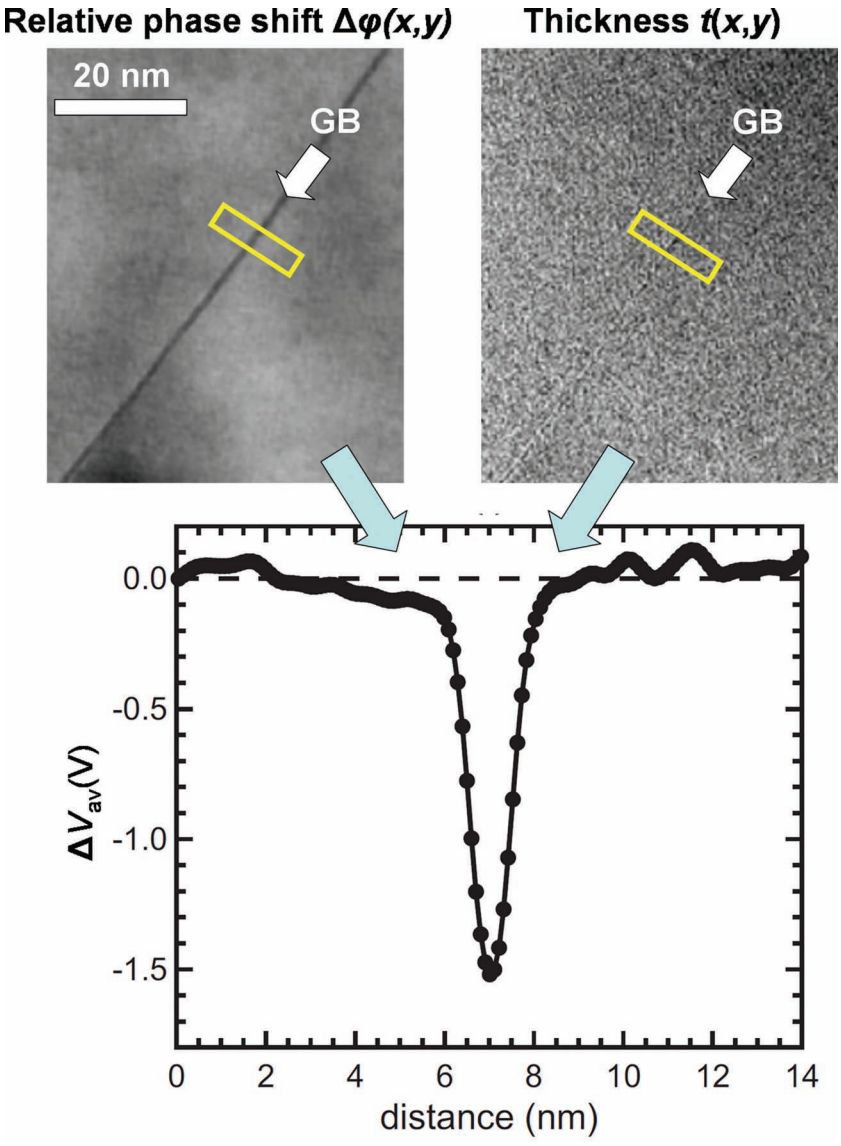

Figure 1. Relative phase shift $\phi(x,y)$ and specimen thickness $t(x,y)$ of the identical area on a Cu(In,Ga)Se_2 thin-film in a completed solar cell. From the regions highlighted by yellow frames, profiles were extracted, and the shown profile of the spatial distribution of the averaged electrostatic potential, $\Delta V_{av}(V)$, across the GB was calculated by use of Equation 1.

charges within the neutral solid, i.e., protons and electrons, and is - because of the higher localization of positive charges - a positive quantity. Changes in MIP can be caused by variations in the (local) composition, in crystal structure and/or in the (local) density.

In ΔV_{av} profiles across GBs, which were extracted from grey value distributions of phase and thickness (Figure 1), potential wells are present at the position of the GBs. For all random GBs analyzed, including other Cu(In,Ga)Se_2 thin-films not presented here, these potential wells exhibited widths of 1–2 nm and depths of 1–3 V. We note that the noise levels around the GBs in the ΔV_{av} images are about 100–200 mV.

We find the contribution of ΔV_{charge} to the potential wells to be rather small. For the underlying estimation, it may be assumed that negative charges are present at the GBs, generating an electric field which is screened into the grain interior by an accumulation of free holes in the *p*-type Cu(In,Ga)Se_2 thin-films, with Debye lengths of $L_{Debye} = \left(\frac{\varepsilon_0 \varepsilon_{CIGSe} k_B T}{e^2 p}\right)^{1/2}$, ε_0 and ε_{CIGSe} being the dielectric permittivity of the vacuum and of Cu(In,Ga)Se_2, k_B the Boltzmann constant, T the absolute temperature, e the elemental charge, and p the effective doping of Cu(In,Ga)Se_2. Such a configuration can indeed cause potential wells. However, with $\varepsilon_{CIGSe} = 12$ and $p = 10^{16}$–10^{17} cm^{-3}, the Debye length can be calculated to be about 10–40 nm, which is an order of magnitude larger than the 1–2 nm widths of the measured potential wells. In this estimation, one must consider that the incident electron beam in the TEM generates additional free charge-carriers during the measurement, which may be on the order of magnitude of the doping density of the semiconductor. However, such a generation of free charge-carriers was avoided by using appropriate illumination conditions.

Also, the possibility of positive charges screened by a negative space-charge region can be neglected, since this scenario would lead to electrostatic potential barriers (as experienced by the impinging electron beam) and not to potential wells (as measured here).

Overall, we can not exclude the presence of charge densities at GBs, leading to a band bending of a few 100 meV since the corresponding potential distributions occur in a field of view that cannot be detected with the applied method of in-line electron holography, which is limited to a length scale of about 20 nm perpendicular to the GB, related to the lateral coherence length of the electron beam.

It should be noted that the reduced average electrostatic potentials at GBs may also be due to the presence of surface grooves in the TEM specimen. So far, we have not been able to detect such surface grooves (by use of thickness measurements in the TEM). Therefore, it is likely that the main contribution to the electrostatic potential wells found at GBs in Cu(In,Ga)Se_2 thin-films are variations in the mean-inner potential ΔMIP and, thus, in density or in composition. The mass density at GBs may be reduced simply because of the fact that the periodic lattices of the adjacent grains do not fit well, i.e., large densities of spacing between atomic columns remain.

Indeed, we were able to relate the electrostatic potential wells at Cu(In,Ga)Se_2 GBs directly to changes in composition. Profiles of ΔV_{av} and profiles evaluated from element-sensitive EELS measurements in a scanning TEM, both obtained across the identical GB in a Cu(In,Ga)Se_2 thin-film are given in **Figure 2**. It can be seen that the In and O signals are enhanced, whereas the Cu and Se signals exhibit minima at the position of the GB (note that O may also be introduced in part during the TEM

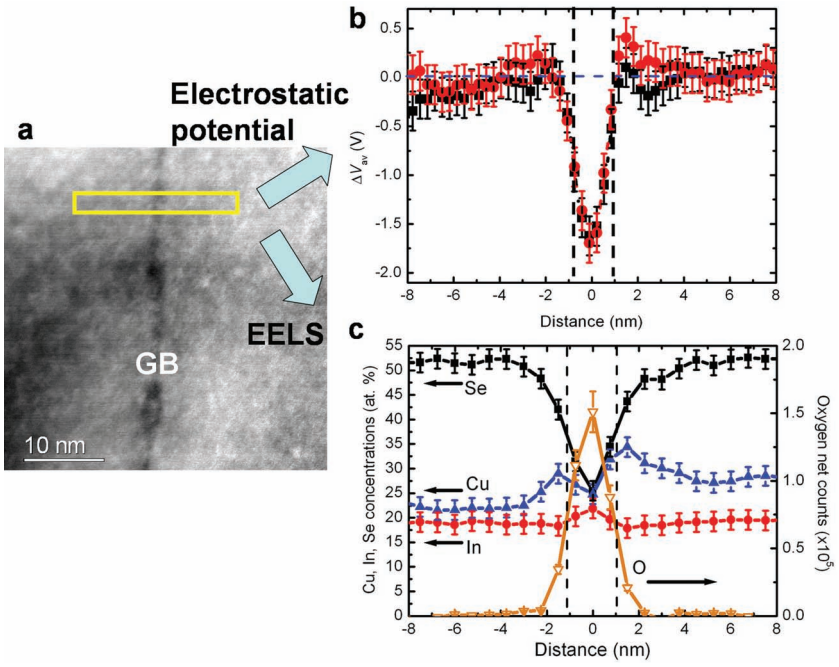

Figure 2. a) High-angle annular dark-field image of a position containing a random (non-twin) GBs (the dark spots are related to carbon contaminations). Across this GB, distributions of the electrostatic potentials (b) were obtained (where these two profiles were acquired at two different positions on this GB), as well as elemental distribution profiles by means of EELS (c). The region of change in electrostatic potential and in composition is confined to 1–2 nm. The measured potential wells can be attributed directly to a change in composition. Enrichment of In and O as well as depletion of Cu and Se were detected. The errors of measurement for the electrostatic potential were assumed to be about 0.2 V, those of the Cu, In, and Se concentrations were quantified by integral XRF analysis of the Cu(In,Ga)Se_2 thin-film as about 2 at%, and the errors for the oxygen net counts were about 10% relative to the corresponding values.

specimen preparation). The Ga–L edge in the EEL spectrum was superimposed on the Cu–L edge, and was therefore not evaluated. It was also not possible to detect Na signals above the noise level. We note that we find both increased and decreased elemental concentrations at the GB. Therefore, the electrostatic potential wells we measured can not be interpreted in terms of only reduced mass density at the GB, but certainly the reduced density has an impact on the presence of the potential wells. This issue is discussed in more detail elsewhere.[16] We also would like to mention that the result of Cu depletion and In enrichment has been reported by Hetzer al.,[17] who found this behaviour at a large number of Cu(In,Ga)Se_2 GBs applying very surface-sensitive Auger electron spectroscopy.

The widths of the minima and maxima in the EELS signals match the width of the electrostatic potential wells (1–2 nm). By assuming isolated atoms or ions, at which the incident electron in the TEM scatters, the MIP may be approximated by[18] $\mathrm{MIP} = \left(\frac{h^2}{2\pi m e \Omega}\right) \sum_{\text{unit cell}} f_{\text{el}}(0)$ (Equation 2), where h is Planck's constant, m the mass of the electron, e the elemental charge, Ω the volume of the unit cell, and $f_{\text{el}}(0)$ the atomic or ionic scattering factor at zero scattering angle. Using the concentrations of Cu, In, and Se (Figure 2) as well as the resulting concentration of Ga (assuming [Cu] + [In] + [Ga] + [Se] = 1 integrally in the Cu(In,Ga)Se_2 layer, which is not given at the GB in view of the O signal and other impurities possibly being present), their corresponding scattering factors,[18] and the lattice constants for the tetragonal crystal structures of $CuInSe_2$[19] and of $CuGaSe_2$,[20] the resulting change in MIP was calculated by use of Equation 2. With the compositional changes given in Figure 2, we are able to estimate a lowering of the MIP of about 3.3 V, which is in good agreement with the depths of the measured potential wells of about 1.6–1.8 V. The discrepancy can be explained by assuming that additional O, which was not considered in the estimation, and other impurities increase the MIP such that the depth of the potential wells becomes about 1.6–1.8 V.

Figure 3 shows results obtained again acquiring EELS elemental distribution electrostatic potential profiles, on a different GB to that in Figure 2 (however, still in the identical Cu(In,Ga)Se_2 thin film). Although again potential wells are found at this GB, Cu enrichment and In depletion was measured, in addition to increased O and decreased Se concentrations. It is apparent from the data in Figure 3c that the Cu and In as well as the Se and O signals are anticorrelated. Here, a lowering of the MIP of 1.2 V is obtained from the EELS results (Figure 3c), again agreeing well with the experimental data given in Figure 3b. Additional EELS measurements indicate that the dark spots visible at the GB in Figure 3a are precipitates depleted in Se and In and enriched in O and Cu (this is, similar as at the GB). Dislocations at this GB were not identified in TEM images when tilting the specimen in order to orient the GB edge-on for the electron holography measurement.

The EELS results given above in Figures 2 and 3 already indicate that the compositions of random Cu(In,Ga)Se_2 GBs can vary strongly and that there is not any general trend. This finding is corroborated by **Figure 4**, which gives elemental distribution profiles obtained by APT, acquired across a GB in the same Cu(In,Ga)Se_2 thin-film as the EELS measurements. Being a mass spectrometry technique, APT also allows for the detection of trace elements apart from the matrix elements in Cu(In,Ga)Se_2. In contrast to the EELS data in Figure 2, but in agreement with that given in Figure 3, the Cu signal is enhanced at this GB, whereas that of In is reduced. The Ga and Se concentrations exhibit minima, and Na, K, H, and O are apparently enriched at the GB. While Na enrichments at GBs in Cu(In,Ga)Se_2 have already been published by several other authors[21–23], further previous work[23,24] has shown additionally also enhanced O and K signals. Na, O and K are present as Na_2O and K_2O in the soda-lime glass used as substrate for the solar-cell stack, probably diffusing into Cu(In,Ga)Se_2 during the growth process,[25] whereas H may stem from the residual gas in the APT instrument.

The widths of the GB regions, where changes in composition and in the average electrostatic potential were measured,

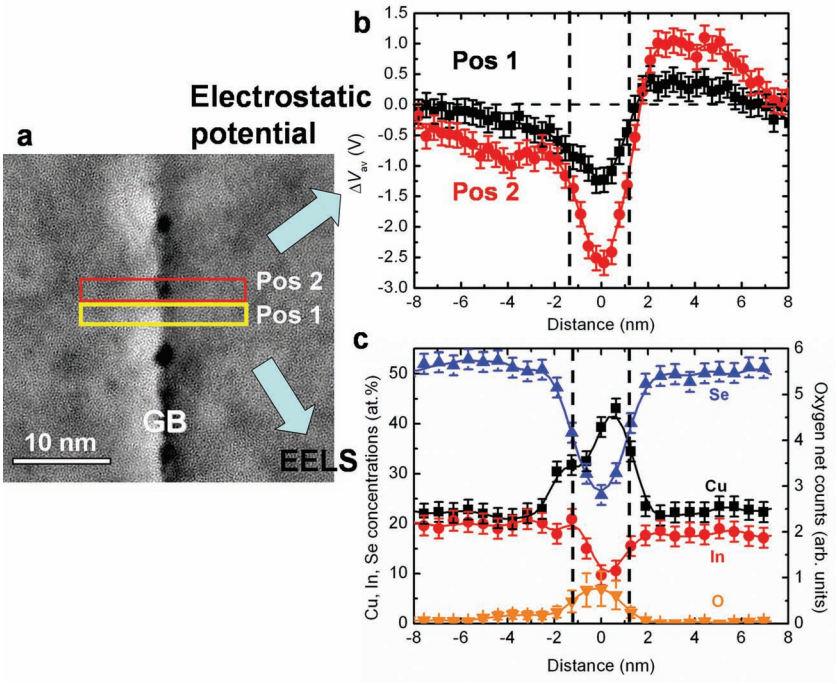

Figure 3. a) Phase image of a position containing a random (non-twin) GB. Across this GB, linescans of the electrostatic potentials at positions 1 (same as EELS linescan) and 2 (across dark spot) were obtained (b), as well as elemental distribution profiles by means of EELS at position 1 (c). The region of change in electrostatic potential and in composition is confined to slightly more than the 1–2 nm in Figure 2. The asymmetric shapes of the potentials and also the elemental distribution profiles can be attributed to a slightly inclined GB (which could not be corrected by tilting the specimen). As in Figure 2, the measured potential well can be attributed directly to a change in composition. Enrichment of Cu and O as well as depletion of In and Se were detected. The errors of measurement are the same as in Figure 2.

are – consistently for all measurement techniques applied: only about 1–2 nm. In a different work,[26] we have shown that these widths can be as small as 0.7 nm. That is, the change in composition occurs only within the atomic planes nearest to the GB core. This extension is too small to correlate with secondary phases. Rather, it should be considered as a local atomic redistribution confined to few interatomic distances. The larger widths of 1–2 nm of the GB regions measured in this work are attributed to the fact that random GBs are in general not planar surfaces, which, owing to the fact that only the projection of the electrostatic potential can be measured, results in smeared out signals broader than the actual extension.

We performed further EELS and APT analyses at GBs in $Cu(In,Ga)Se_2$ thin-films with various compositions and growth conditions (data not given here), where we found compositional changes once more differing from those given above. The Se concentration is sometimes increased, sometimes decreased or sometimes does not change significantly. The Ga signal does not always show the same behavior as the In signal, and for some GBs it does not change significantly. At most GBs analyzed, Na and O are enriched. Based on numerous measurements by EELS and APT, we can exclude the variety of compositional changes at GBs being due to measurement artefacts. We would like to note that the result of always different compositional changes at different $Cu(In,Ga)Se_2$ GBs can be related to the result of different band bending at different GBs, as reported by Baier et al.,[27] who performed scanning Kelvin probe force microscopy combined with EBSD at identical positions.

Although there is no clear trend for the compositional changes at different GBs, all EELS and APT results have one detail in common. If the Cu signal is increased at the GB, the In signal is reduced, and vice versa. This anticorrelation of the Cu and the In concentrations is a strong indication of atomic redistribution at the GBs; this is because almost all atomic planes in the tetragonal $Cu(In,Ga)Se_2$ crystal structure are occupied by Cu and In (and Ga) (only the {101} planes contain either only Cu or only In (and Ga) atoms). Thus, depletion of Cu or In can not be explained by geometrical effects at the GB (assuming that not all random GB coincidentally consist of two grains terminated by{101} planes facing each other, which can be excluded owing to the curvature of the analyzed GBs and the lattice structure within high-resolution STEM images at GBs) but again only by atomic redistribution. In this case, the compound semiconductor $Cu(In,Ga)Se_2$ seems to provide a unique chemical flexibility for this atomic redistribution in a very confined region.

This result of different changes in composition with anticorrelated Cu and In signals at various GBs in $Cu(In,Ga)Se_2$ thin films gives rise to a novel GB model, which is outlined in the following. It is important at this point to note that for high-efficient, thin-film solar cells, non-stoichiometric $Cu(In,Ga)Se_2$ layers are used, with typical concentration ratios of [Cu]/([In] + [Ga]) = 0.8–0.9. A certain fraction of the Cu sites in the chalcopyrite-type lattice (depending on the deposition recipe of the $Cu(In,Ga)Se_2$ thin film under investigation) are vacancies (see **Figure 5**). This is one reason why Cu exhibits a high mobility in $Cu(In,Ga)Se_2$ thin-films,[28] which also promotes the formation of In_{Cu}^{2+} and Ga_{Cu}^{2+} point defects.

As listed in Figure 5, the number of intrinsic and impurity-induced defects is rather large. V_{Cu}^{-}, Cu_{In}^{2-}, and Cu_{Ga}^{2-} may lead to acceptor states in the electronic band gap, whereas V_{Se}^{2+}, In_{Cu}^{2+}, and Ga_{Cu}^{2+} give rise to donors. Moreover, it was shown[29] that the defect pairs ($2V_{Cu}^{-} + In_{Cu}^{2+}$) and ($Cu_{In}^{2-} + In_{Cu}^{2+}$) have particularly low formation enthalpies. Considering the striking anticorrelation of all Cu and In signals at $Cu(In,Ga)Se_2$ GBs found in numerous measurements, it may be that the concentrations of these neutral defect complexes are particularly high at $Cu(In,Ga)Se_2$ GBs.

Segregation of the impurities Na, K, and O at GBs implies the formation of the impurity-induced point defects Na_{Cu}, K_{Cu}, and O_{Se}, which are quasi-neutral but result in the formation of weak donors and weak acceptors because of the different electronegativities of O and Se as well as of Na, K, and Cu. The overall

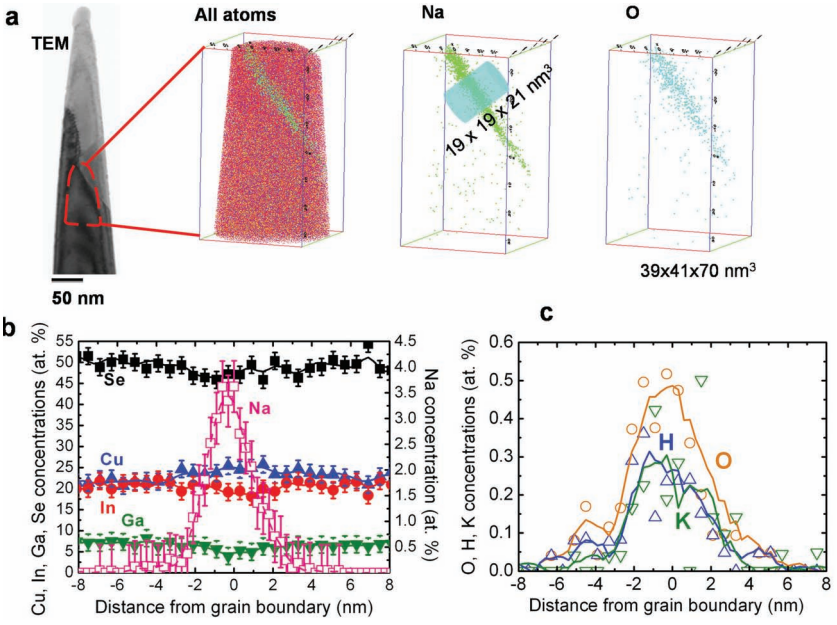

Figure 4. Results from atom-probe tomography performed on a $Cu(In,Ga)Se_2$ thin-film. a) Bright-field TEM image of the tip containing a GB (identified by diffraction contrast), as well as corresponding reconstructed, three-dimensional data cube giving the elemental distributions by false colors. Extracted elemental distribution profiles from this data cube are given in (b) for Cu (blue up triangles), In (red circles), Ga (green down triangles), Se (black full squares), and Na (pink open squares), as well as in (c) for O (yellow open circles), H (blue open triangles), and K (green open triangles). All lines are guides for the eyes. The errors of the concentrations in (b) were estimated to about 2 at% (Cu, In, Ga, Se) and to about 0.5 at% (Na). In c), no error bars are given to provide better visibility of the data; however, the scattering of the raw data in this viewgraph is apparent.

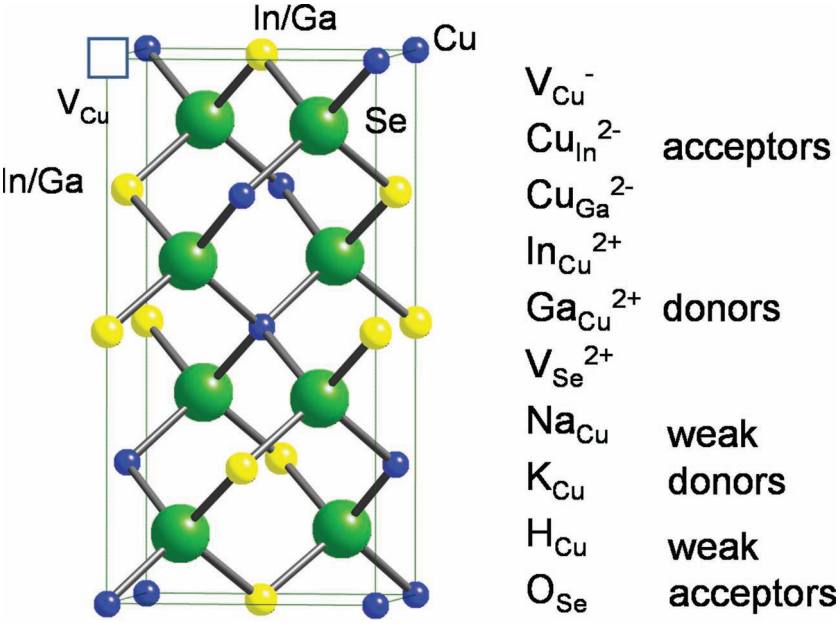

Figure 5. Unit cell of the tetragonal, chalcopyrite-type crystal structure of $Cu(In,Ga)Se_2$, comprising vacancies on the Cu sites. Intrinsic point defects and those induced by impurities are listed, indicating whether they are expected to form donor or acceptor states.

GB energy can be lowered by atomic or ionic redistribution in atomic planes adjacent to the GB core. Since different growth conditions and different densities of segregated impurities (due to different glass substrates used or due to different growth recipes applied) can result in various situations at GBs in $Cu(In,Ga)Se_2$ layers, the atomic/ionic redistribution is not equal for all GBs. Therefore, the GBs differ in general in their compositions, i.e., for differently grown and also within identical $Cu(In,Ga)Se_2$ thin films.

Consequences for an electronic band diagram in the vicinity of a $Cu(In,Ga)Se_2$ GB are difficult to detail. The point defects V_{Cu}^{-}, Cu_{In}^{2-} and Cu_{Ga}^{2-} as well as V_{Se}^{2+}, In_{Cu}^{2+} and Ga_{Cu}^{2+} are also present in the grain interiors,[30,31] forming acceptor and donor states in the bandgap, making $Cu(In,Ga)Se_2$ a highly compensated semiconductor. According to the considerations given above, their densities are increased at the GBs. Assuming varying compositional changes at different GBs, the band diagrams are expected to exhibit various "band offsets" in conduction and valence bands at the positions of the GBs.

The model of confined and chemically flexible GBs in this work cannot exclude any of the various other GB models for $Cu(In,Ga)Se_2$ thin films reported in the literature. Charge accumulation at $Cu(In,Ga)Se_2$ GBs[32–37] has to be considered.

Atomic reconstruction at $Cu(In,Ga)Se_2$ GBs has already been suggested by Persson and Zunger[38] based on density functional theory (DFT) calculations on highly symmetric Σ3 twin GBs. However, these authors predict the formation of Cu vacancies or In_{Cu}^{2+} antisite defects, while we found various changes in Cu and In concentrations, and also further compositional variations. The confinement of the GB to only about 1 nm in width is closely related to the neutral (tunnelling) barrier proposed by Azulay et al.[39] as well as by Hafemeister et al.,[40] except that the negative valence-band offset proposed by these authors is again most probably not found at all GBs. A (quasi)-charge-neutral GB without (or with hardly) any band bending or band offset was suggested by Yan et al.[41] From DFT calculations, these authors suggest very low densities of deep defects in the band gap (for which experimental evidence has been provided by Moenig et al.[42]) due to lattice relaxations, which can be related to the atomic/ionic redistributions found in this work. This is a good explanation for the low recombination velocities measured at $Cu(In,Ga)Se_2$ GBs.[5] Although atomic redistibution may compensate for charge at the GBs, it cannot be concluded from the results given here that charge neutrality is a general feature of a $Cu(In,Ga)Se_2$ GB.

4. Conclusion

It has been shown directly that the regions of the GBs in $Cu(In,Ga)Se_2$ thin-films where changes in composition occur are strongly confined to only about 1 nm in width, i.e., to the atomic planes nearest to the GB core. This result was corroborated by distributions of the averaged electrostatic potential and by EELS linescans, both acquired on the identical positions, as well as by APT measurements. Therefore, the changes in composition are due to atomic/ionic redistribution in the neighboring atomic planes. The changes in composition and therefore the atomic/ionic reconstruction were found to be different for different GBs in various $Cu(In,Ga)Se_2$ thin films. We emphasize that only by application of techniques with resolutions on the subnanometer scale, as employed here, can the compositional changes at $Cu(In,Ga)Se_2$ GBs be detected. The correlation between the electrostatic potential wells and the local compositional changes we found at GBs and their electronic properties has to be examined further by DFT calculations.

Acknowledgements

The authors would like to thank B. Bunn, C. Kelch, M. Kirsch, and T. Münchenberg for help in solar-cell preparation, as well as J. Bundesmann, H. Stapel, and M. Wollgarten for scientific and technical assistance with the electron microscopes. Funding from the German Ministry for Environment (BMU) under contract #0327559H (German-Israeli project ProGraB) as well as by the ESTEEM project is gratefully acknowledged. BS and MS thank the EPSRC for funding of the SuperSTEM facility and for operator time. Special thanks are due to H. Kropf, HZB, for FIB preparation and to Dr. B. Mendis, Durham University, for providing access to an FIB machine.

Received: December 18, 2011
Published online: May 10, 2012

[1] I. Repins, M. A. Contreras, B. Egaas, C. DeHart, J. Scharf, C. L. Perkins, B. To, R. Noufi, *Prog. Photovoltaics Res. Appl.* **2008**, *16*, 235.
[2] P. Jackson, D. Hariskos, E. Lotter, S. Paetel, R.Wuerz, R. Menner, W. Wischmann, M. Powalla, *Prog. Photovoltaics Res. Appl.* **2011**, *19*, 894.
[3] P. Jackson, R. Würz, U. Rau, J. Mattheis, M. Kurth, T. Schlötzer, G. Bilger, J. H. Werner, *Prog. Photovoltaics Res. Appl.* **2007**, *15*, 507.
[4] D. Abou-Ras, R. Caballero, C. A. Kaufmann, M. Nichterwitz, K. Sakurai, S. Schorr, T. Unold, H. W. Schock, *Phys. Status Solidi RRL* **2008**, *2*, 135.
[5] M. Nichterwitz, D. Abou-Ras, K. Sakurai, J. Bundesmann, T. Unold, R. Scheer, H. W. Schock, *Thin Solid Films* **2009**, *517*, 2554
[6] C. Donolato, *Mater. Sci. Eng. B* **1996**, *42*, 306.
[7] S. Sadewasser, D. Abou-Ras, D. Azulay, R. Baier, I. Balberg, D. Cahen, S. Cohen, K. Gartsman, K. Ganesan, J. Kavalakkatt, W. Li, O. Millo, T. Rissom, Y. Rosenwaks, H.-W. Schock, A. Schwarzman, T. Unold, *Thin Solid Films* **2011**, *519*, 7341.
[8] S. Bhattacharyya, C. T. Koch, M. Ruehle, *Ultramicroscopy* **2006**, *106*, 525.
[9] C. T. Koch, *Ultramicroscopy* **2008**, *108*, 141.
[10] R. E. Dunin-Burkowski, *Ultramicroscopy* **2000**,*83*, 193.
[11] M. Schaffer, B. Schaffer, Q. Ramasse, *Ultramicroscopy* **2012**, *114*, 62.
[12] K. Sader, B. Schaffer, G. Vaughan, R. Brydson, A. Brown, A. Bleloch, *Ultramicroscopy 110*, 998.
[13] M. K. Miller, K. F. Russell, K. Thompson, R. Alvis, D. J. Larson, *Microsc. Microanal.* **2007**, *13*, 428.
[14] D. B. Williams, C. B. Carter, *Transmission Electron Microscopy, A Textbook for Materials Science*, Springer Science and Business Media, New York, London **2009**.
[15] R. F. Egerton, *Electron Energy-Loss Spectroscopy in the Electron Microscope* Plenum Press, New York **1996**.
[16] S. S. Schmidt, PhD Thesis, TU Berlin**2011**.
[17] M. J. Hetzer, Y. M. Strzhemechny, M. Gao, M. C. Contreras, A. Zunger, L. J. Brillson, *Appl. Phys. Lett.* **2005**, *86*, 162105.
[18] D. Rez, P. Rez, I. Grant, *Acta Crystallogr., Sect. A* **1994**, *50*, 481.
[19] K. S. Knight, *Mater. Res. Bull.* **1992**, *27*, 161.
[20] S. C. Abrahams, J. L. Bernstein, *J. Chem. Phys.* **1974**, *61*, 1140.
[21] E. Cadel, N. Barreau, J. Kessler, P. Pareige, *Acta Mater.* **2010**, *58*, 2634.
[22] R. Schlesiger, C. Oberdorfer, R. Würz, G. Greiwe, P. Stender, M. Artmeier, P. Pelka, F. Spaleck, G. Schmitz, *Rev. Sci. Instr.* **2010**, *81*, 043703.
[23] O. Cojocaru-Mirédin, P. Choi, R. Wuerz, D. Raabe, *Ultramicroscopy* **2011**, *111*, 552.
[24] O. Cojocaru-Mirédin, P. Choi, D. Abou-Ras, S. S. Schmidt, R. Caballero, D. Raabe, *J. Photovoltaics* **2011**,*1*, 207.
[25] M. A. Contreras, B. Egaas, P. Dippo, J. Webb, J. Granata, K. Ramanathan, S. Asher, A. Swartzlander, R. Noufi, *Conference Records of the 26th IEEE Photovoltaic Specialists Conference and Exhibition*, IEEE, USA **1997** , p.359
[26] D. Abou-Ras, B. Schaffer, M. Schaffer, S. S Schmidt, R. Caballero, T. Unold, *Phys. Rev. Lett.* **2012**, *108*, 075502.
[27] R. Baier, D. Abou-Ras, T. Rissom, M. C. Lux-Steiner, S. Sadewasser, *Appl. Phys. Lett.* **2011**. **99** , 172102
[28] K. Gartsman, L. Chernyak, V. Lyahovitskaya, D. Cahen, V. Didik, V. Kozlovsky, R. Malkovich, E. Skoryatina, V. Usacheva, *J. Appl. Phys.* **1997**, *82*, 4282.
[29] S. B. Zhang, S.-H. Wei, A. Zunger, H. Katayama-Yoshida, *Phys. Rev. B* **1998**, *57*, 9642.
[30] G. Dagan, F. Abou-Elfotouh, D. J. Dunlavy, R. J. Matson, D. Cahen, *Chem. Mater.* **1990**, *2*, 286.
[31] I. Dirnstorfer, M. Wagner, D. M. Hofmann, M. D. Lampert, F. Karg, B. K. Meyer, *Phys. Status Solidi A* **1998**, *168*, 163.
[32] J. Y. W. Seto, *J. Appl. Phys.* **1975**, *46*, 5247.
[33] S. Schuler, S. Nishiwaki, J. Beckmann, N. Rega, S. Brehme, S. Siebentritt, M. C. Lux-Steiner, *Conference Records of the 29th IEEE Photovoltaic Specialists Conference*, IEEE, USA **2002**, p.504.
[34] S. Siebentritt, S. Schuler, *J. Phys. Chem. Solids* **2003**, *64*, 1621.
[35] S. Sadewasser, T. Glatzel, S. Schuler, S. Nishiwaki, R. Kaigawa, M. C. Lux-Steiner, *Thin Solid Films* **2003**, *257*, 431.
[36] C.-S. Jiang, R. Noufi, J. A. AbuShama, K. Ramanathan, H. Moutinho, J. Pankow, M. M. Al-Jassim, *Appl. Phys. Lett.* **2004**, *84*, 3477.
[37] D. Fuertes Marron, S. Sadewasser, A. Meeder, T. Glatzel, M. C. Lux-Steiner, *Phys. Rev. B* **2005**, *71*, 033306.
[38] a) C. Persson, A. Zunger, *Phys. Rev. Lett.* **2003**, *91*, 266401; b) C. Persson, A. Zunger, *Appl. Phys. Lett.* **2005**, *87*, 211904.
[39] D. Azulay, O. Millo, I. Balberg, H.-W. Schock, I. Visoly-Fisher, D. Cahen, *Sol. Energy Mater. Sol. Cells* **2007**, *91*, 85.
[40] M. Hafemeister, S. Siebentritt, J. Albert, M. C. Lux-Steiner, S. Sadewasser, *Phys. Rev. Lett.* **2010**, *104*, 196602.
[41] Y. Yan, C.-S. Jiang, R. Noufi, S.-H. Wei, H. R. Moutinho, M. M. Al-Jassim, *Phys. Rev. Lett.* **2007**, *99*, 235504.
[42] H. Moenig, Y. Smith, R. Caballero, C. A. Kaufmann, I. Lauermann, M. C. Lux-Steiner, S. Sadewasser, *Phys. Rev. Lett.* **2010**, *105*, 116802.